International Journal of Multiphase Flow 35 (2009) 185–194

Contents lists available at ScienceDirect

International Journal of Multiphase Flow

journal homepage: www.elsevier.com/locate/ijmulflow

Multiphase Euler–Lagrange CFD simulation applied to Wet Flue Gas Desulphurisation technology

Luca Marocco [a,*], Fabio Inzoli [b]

[a] Independent Researcher, via Luigi Barzini, 18, 20125 Milano, Italy
[b] Department of Energy, Politecnico di Milano, P.zza Leonardo da Vinci, 32, 20133 Milano, Italy

ARTICLE INFO

Article history:
Received 13 July 2008
Received in revised form 8 September 2008
Accepted 14 September 2008
Available online 15 October 2008

Keywords:
CFD
Desulphurisation
Absorption
Multiphase

ABSTRACT

The gas and liquid hydrodynamics inside an Open Spray Tower has been simulated using a commercial CFD code, while a model that treats the absorption process of SO_2 has been developed and implemented in the software through dedicated modules. Besides SO_2 absorption also evaporation of slurry droplets and droplet-wall interaction are considered, the latter modeled with an empirical correlation and implemented in a sub-module.

The continuous gas phase has been modeled in an Eulerian framework, while the dispersed liquid phase with a Lagrangian approach by tracking a large number of particles through the computational domain. Physical absorption of SO_2 has been modeled using dual-film theory and appropriate empirical and semi-empirical correlations. The model for aqueous phase chemistry considers instantaneous equilibrium reactions of eight dissolved species into a slurry droplet, namely: $SO_{2,aq}$, $CO_{2,aq}$, H^+, OH^-, HSO_3^-, SO_3^{2-}, HCO_3^-, CO_3^{2-}. The empirical droplet-wall interaction model handles impact, deposition and splashing events occurring when a liquid particle hits an internal element of the scrubber. A pilot plant OST has been simulated and the numerical results show good agreement with the experimental values of pressure drop, temperature and sulphur dioxide removal efficiency.

1. Introduction

Sulfur dioxide removal from flue gases has probably been the subject of more research than any other gas purification operation. Since the vast majority of SO_2 emissions are from fossil fuel-fired boilers at power stations, these sources have been widely controlled. The limestone forced oxidation system is the most extensively used wet scrubbing process in the world today, comprising roughly one third of the wet scrubbing systems and has been the subject of numerous studies and publications (Klingspor and Cope, 1987). Among the available desulphurisation equipments, Open Spray Towers (OST) are the most frequently installed scrubber types for limestone Wet Flue Gas Desulphurization (WFGD) plants and they cover the major part of the market today.

In the last decade and especially in Europe, the SO_2 emissions regulation has become more stringent necessitating very high scrubbing performances, only achievable through optimization of the WFGD equipment design. This is nowadays mainly based on empirical and/or semi-empirical correlations between process parameters that can be easily measured and controlled. Previous CFD studies (Heiting et al., 2004; Hofelsauer et al., 2008) are limited to the analysis of the gas and liquid hydrodynamics inside an OST. Sulphur dioxide removal efficiency is a complex function of chemistry and fluid dynamics and can be properly evaluated with the model developed in this work, which computes the local and global SO_2 mass transfer between the gas and liquid phase.

Different simulations of a pilot plant OST have been performed. The CFD code ANSYS-FLUENT 6.3.26 has been used to simulate the gas–liquid hydrodynamics, while the developed model has been implemented in the software through dedicated modules. Furthermore, besides SO_2 absorption, the model also simulates evaporation of slurry droplets and droplet-wall interaction, the latter modeled with an empirical correlation and implemented in a sub-module.

The numerical results obtained with three different grid discretizations have been analyzed and compared with the measured data.

2. Governing equations

The fluid dynamics inside an OST can be described as a two-phase flow consisting of a carrier gas and a large number of dispersed liquid droplets and has been modeled with an Euler–Lagrange approach (Lapin and Lübbert, 1994). The main advantage of using a Lagrangian framework for dispersed phase flows is that particle-level phenomena can be modeled rigorously, thus allowing to accommodate complicated forms of interphase physical processes. Furthermore, droplet size distribution and droplet-wall

* Corresponding author. Tel.: +39 328 2321735.
E-mail address: luca.marocco@polimi.it (L. Marocco).

0301-9322/$ - see front matter © 2008 Elsevier Ltd. All rights reserved.
doi:10.1016/j.ijmultiphaseflow.2008.09.005

interaction, both aspects very important in spraying equipment, can be easily taken into account.

2.1. Carrier phase

The flue gas motion in the spray tower is modeled in a fixed frame of reference (Eulerian description).

The liquid volume fraction, α_d, inside an OST is typically lower than 8–10% everywhere, except very close to the spray nozzles. Because this region of high liquid volume fraction is limited to a small portion of the computational domain the following fundamental assumptions are justified:

a) The dispersed liquid phase occupies a low volume fraction and its effects on the continuous phase are negligible, i.e. $\alpha_d \to 0$ or $\alpha_c \to 1$, where α_d and α_c represent the liquid phase and the gas phase volume fraction, respectively.
b) The dispersed phase is sufficiently dilute so that particle–particle interactions are negligible.

Furthermore, the following assumption is valid all through the present work:

c) The dispersed liquid phase consists of spherical droplets.

Following the work of Crowe et al. (1998), and considering the assumptions above, the conservation equations of the continuous phase assume then the same formulation as the conservation equations of a single phase flow with the addition of source terms, which represent mass, S_{mass} and $S_{A,mass}$, momentum, S_{mom}, and energy, S_{en}, coupling between the phases:

$$\frac{\partial}{\partial t}\rho + \nabla\cdot(\rho\mathbf{u}) = S_{mass} \tag{1}$$

$$\frac{\partial}{\partial t}(\rho\mathbf{u}) + \nabla\cdot(\rho\mathbf{u}\otimes\mathbf{u}) = -\nabla p + \nabla\cdot(\tau+\tau^R) + \rho\mathbf{g} + S_{mom} \tag{2}$$

$$\frac{\partial}{\partial t}(\rho i) + \nabla\cdot(\rho\mathbf{u} i) = -p\nabla\cdot\mathbf{u} + \nabla\cdot(k_c\nabla T) + \rho\mathbf{u}\mathbf{g} + S_{en} \tag{3}$$

$$\frac{\partial}{\partial t}(\rho\omega_A) + \nabla\cdot(\rho\omega_A\mathbf{u}) = \nabla\cdot(\rho D_{AB}\nabla\omega_A) + S_{A,mass} \tag{4}$$

The above equations are valid for spherical, non-rotating droplets; ρ is the flue gas density, p the flue gas pressure, $\mathbf{g}$ the acceleration of gravity vector, $\mathbf{u}$ and $\mathbf{v}$ the flue gas and droplet velocity vector, respectively, T the flue gas temperature, τ and τ^R are the shear stress and Reynolds stress tensor, respectively, i is the internal energy per unit mass, ω_A is the mass fraction of component A, D_{AB} is the binary diffusion coefficient of species A in B and k_c is the continuous phase thermal conductivity.

Turbulence energy and dissipation rate can be affected by the presence of dispersed particles. This effect is known as *turbulence modulation*. Source terms should be added in the equations of k and ε to account for turbulence modulation. Anyway, there is experimental evidence that modulation is weak if the particle concentration is very low, i.e. if $\alpha_d \to 0$. Therefore, the k–ε realizable model has been used in its formulation for single-phase flows (Launder and Spalding, 1972; Shih et al., 1995).

The source terms S_{mass}, S_{mom}, S_{en} and $S_{A,mass}$ are calculated by volume averaging the contributions from all the individual droplets within the cell volume (Crowe et al., 1998).

$$S_{mass} = -\frac{1}{V}\sum_k \dot{m}_k \tag{5}$$

$$S_{mom} = -\frac{1}{V}\sum_k \mathbf{v}_k\dot{m}_k - \frac{1}{V}\sum_{i,k}\mathbf{F}_{i,k} \tag{6}$$

$$S_{en} = -\frac{1}{V}\sum_{i,k}\mathbf{F}_{i,k}\mathbf{v}_k - \frac{1}{V}\sum_k \dot{m}_k h_{lv,A} + \frac{1}{V}\sum_k \dot{Q}_k \tag{7}$$

$$S_{A,mass} = -\frac{1}{V}\sum_k \dot{m}_{A,k} \tag{8}$$

where the subscript k refers to the kth droplet, $\mathbf{v}$ is the droplet's velocity vector, $F_{i,k}$ is the sum of the forces acting at the interface between the phases, $h_{lv,A}$ is the latent heat of vaporization of component A and $\dot{Q}_k$ is the convective heat transfer between phases.

After evaluation of these source terms, the gas phase conservation equations need to be solved again (*two-way coupling*). The resulting flow, temperature and concentration fields are then used to calculate updated source terms and so on until convergence.

2.2. Dispersed phase

Once the gas velocity field is known, the particles' trajectories can be computed. The dispersed liquid phase is calculated with a Lagrangian approach by tracking a large number of particles, called *parcels*, through the computational domain. The equations of motion of a single parcel take the following form:

$$\frac{d\mathbf{x}}{dt} = \mathbf{v} \tag{9}$$

$$\frac{dm_d}{dt} = S_{k,mass} \tag{10}$$

$$m_d\frac{d\mathbf{v}}{dt} = S_{k,mom} + m_d\mathbf{g} \tag{11}$$

$$m_d c_d\frac{dT_d}{dt} = S_{k,en} \tag{12}$$

The subscript d indicates that the quantity is referred to a droplet and c is the droplet's specific heat.

Starting from injection conditions specified for each nozzle, these ordinary differential equations are solved by stepwise integration over discrete time steps, using the continuous phase flow properties at the current droplet position.

3. Source terms

The evaluation of the particle's source terms in Eqs. (10)–(12), for a spherical non-rotating droplet, allows the determination of the source terms in the gas phase flow equations.

3.1. Momentum source term

According to Eq. (6), momentum is exchanged between phases through mass transfer and interphase forces.

The determination of the momentum source term associated with mass exchange follows from the calculation of mass transfer between phases.

The motion of an *isolated* particle inside the computational domain can be described through the Basset–Boussinesq–Oseen (BBO) equation. The momentum source term in Eq. (11) is the sum of the forces acting on a particle.

According to Crowe et al. (1998), Eq. (11) can be written as:

$$m_d\frac{d\mathbf{v}}{dt} = \frac{1}{2}\rho C_D|\mathbf{u}-\mathbf{v}|(\mathbf{u}-\mathbf{v})A_d + m_d\mathbf{g} + O\left(\frac{\rho}{\rho_d}\right) \tag{13}$$

Therefore, in gas–liquid flows where the above density ratio is low, the only two important forces that significantly contribute to the particle's linear momentum variation are the *steady-state drag force* and the *gravity force*.

Table 1
Summary of the differential form of the conservation equations for the carrier gas phase of a dispersed two-phase gas–liquid flow.

	Conservation equation	Source terms
Continuity	$\frac{\partial}{\partial t}\rho + \nabla\cdot(\rho\mathbf{u}) = S_{\text{mass}}$	$S_{\text{mass}} = -\frac{1}{V}\sum_k \dot{m}_k$
Momentum	$\frac{\partial}{\partial t}\rho\mathbf{u} + \nabla\cdot(\rho\mathbf{u}\otimes\mathbf{u}) = -\nabla p + \nabla\cdot(\tau+\tau^{\text{R}}) + \rho\mathbf{g} + S_{\text{mom}}$	$S_{\text{mom}} = -\frac{1}{V}\sum_k \mathbf{v}_k\dot{m}_k - \frac{3\pi\mu}{V}\sum_k D_k f_k(\mathbf{u}-\mathbf{v}_k)$
Energy	$\frac{\partial}{\partial t}(\rho i) + \nabla\cdot(\rho\mathbf{u}i) = -p\nabla\cdot\mathbf{u} + \nabla\cdot(k_c\nabla T) + S_{\text{en}}$	$S_{\text{en}} = -\frac{1}{V}\sum_k \dot{m}_{k,\text{H}_2\text{O}} h_{\text{lv},\text{H}_2\text{O}} + \frac{\pi k_c}{V}\sum_k (\text{Nu}_k) D_k (T_{\text{d},k} - T)$
Species	$\frac{\partial}{\partial t}(\rho\omega_{\text{A}}) + \nabla\cdot(\rho\omega_{\text{A}}\mathbf{u}) = \nabla\cdot(\rho D_{\text{AB}}\nabla\omega_{\text{A}}) + S_{\text{A,mass}}$	$S_{\text{A,mass}} = -\frac{1}{V}\sum_k \dot{m}_{\text{A},k}$

The drag coefficient, C_{D}, is evaluated through the Morsi and Alexander (1972) correlation, that adjusts the value of C_{D} for a spherical particle over a wide range of relative Reynolds numbers, $\text{Re}_{\text{r}} = \rho D|\mathbf{u}-\mathbf{v}|/\mu$:

$$C_{\text{D}} = \text{a}_1 + \frac{a_2}{\text{Re}_{\text{r}}} + \frac{a_3}{\text{Re}_{\text{r}}^2} \tag{14}$$

The coefficients a_i are functions of Re_{r}, D is the droplet's diameter and μ is the flue gas dynamic viscosity.

3.2. Energy source term

Energy is exchanged between phases through mass transfer due to evaporation, $S_{k,\text{evap}}$, and convective heat transfer, $S_{k,\text{conv}}$, while for very dilute flows radiative heat transfer is negligible. The energy source term due to evaporation of water from slurry droplets requires the determination of the rate of mass exchange of water.

The largest droplets' diameters inside an OST are of the order of some millimeters so that droplet's temperature can be considered uniform in the volume. The energy equation (12) for a slurry parcel assumes then the form:

$$m_{\text{d}} c_{\text{d}} \frac{\text{d}T_{\text{d}}}{\text{d}t} = h(T - T_{\text{d}})\pi D^2 + \dot{m}_{\text{d},\text{H}_2\text{O}} h_{\text{lv},\text{H}_2O} \tag{15}$$

The reaction enthalpy of the absorption of sulphur dioxide is negligible compared to the other two energy transfer mechanisms and does not compare in the droplet's heat balance above.

The convective heat transfer coefficient, h, is evaluated with the *Ranz–Marshall* (Ranz and Marshall, 1952) correlation:

$$\text{Nu} = \frac{hD}{k_{\text{c}}} = 2 + 0.6\text{Re}_{\text{r}}^{0.5}\text{Pr}^{0.33} \tag{16}$$

The final form of the gas phase conservation equations is summarized in Table 1.

3.3. Mass source terms

The present study considers *mass transfer of water*, due to evaporation from the slurry droplets to the gas phase, and *absorption of SO_2* from the flue gas mixture into the slurry droplets. Conditions for water vapor condensation and sulphur dioxide desorption hardly occur inside an OST and therefore they have not been considered here. The source term in Eq. (10) can then be written as:

$$S_{k,\text{mass}} = S_{k,\text{H}_2\text{O}} + S_{k,\text{SO}_2} = \dot{m}_{\text{H}_2\text{O}} + \dot{m}_{\text{SO}_2} \tag{17}$$

3.3.1. Evaporation of water

Even though the droplets are a mixture of water, dissolved species and suspended solids, the concentration of water is predominant. The molar flux of water through the interface is then:

$$N_{\text{H}_2\text{O}} = k_{\text{H}_2\text{O,g}}(P_{\text{H}_2\text{O},\infty} - P_{\text{H}_2\text{O,i}}) \tag{18}$$

$P_{\text{H}_2\text{O},\infty}$ is the partial pressure of water in the bulk of the mixture, $P_{\text{H}_2\text{O,i}}$ is the partial pressure of water at droplet's surface and $k_{\text{H}_2\text{O,g}}$ is the gas side mass transfer coefficient.

The partial pressure of water vapor in the gas bulk is known from the solution of the corresponding gas phase species transport equation. The partial pressure of water vapor at droplet's surface is assumed to be equal to the saturated vapor pressure at droplet's temperature and has been approximated with Antoine's equation (Poling et al., 2001). The gas side mass transfer coefficient is evaluated with the *modified Ranz–Marshall* equation (Rowe et al., 1965):

$$\text{Sh} = \frac{k_{\text{H}_2\text{O,g}} DRT}{D_{\text{H}_2\text{O}-\text{ air,g}}} = 2 + 0.69\text{Re}_{\text{r}}^{0.5} Sc^{0.33} \tag{19}$$

In the equation above the binary diffusion coefficient of water vapor in air, $D_{\text{H}_2\text{O}-\text{air,g}}$, is estimated with the *Füller–Schettler–Giddings* equation (Perry and Green, 1998), R is the universal gas constant and T is the flue gas temperature.

3.3.2. SO_2 absorption

Mass transfer of sulphur dioxide involves both gas side and liquid side mass transfer resistances. For low dissolved gas concentration Henry's law can be applied and the molar rate of mass transfer of SO_2, N_{SO_2}, assumes the form:

$$N_{\text{SO}_2} = K_{\text{SO}_2,\text{tot}}(P_{\text{SO}_2,\infty} - H_{\text{SO}_2} C_{\text{SO}_2,\infty}) \tag{20}$$

The global mass transfer coefficient, $K_{\text{SO}_2,\text{tot}}$ is expressed as:

$$\frac{1}{K_{\text{SO}_2,\text{tot}}} = \frac{1}{k_{\text{SO}_2,\text{g}}} + \frac{H_{\text{SO}_2}}{E_{\text{SO}_2} k^0_{\text{SO}_2,\text{l}}} \tag{21}$$

The present work considers conditions far away from the nozzles, where the liquid side mass transfer coefficient in the absence of chemical reactions can be expressed by (Perry and Green (1998)):

$$k^0_{\text{SO}_2,\text{l}} = 10\frac{D_{\text{SO}_2-\text{H,}_2\text{O,l}}}{D} \tag{22}$$

The value of the binary liquid diffusion coefficient of SO_2 in aqueous solution, $D_{\text{SO}_2-\text{H}_2\text{O,l}}$, at 25 °C (Perry and Green, 1998) is extrapolated to the value corresponding to droplet's temperature using the Stokes–Einstein equation:

$$\frac{D_{\text{SO}_2-\text{H}_2\text{O,l}}\mu_{\text{H}_2\text{O}}}{T_{\text{d}}} = \text{const} \tag{23}$$

The enhancement factor, E_{SO_2}, accounts for a higher driving force in the liquid film compared to an absorption without reactions, which are here supposed to occur in the liquid bulk only. According to the work of Brogren and Karlsson (1997) a constant value of the enhancement factor of 10 has been assumed in the present work.

The temperature dependence of Henry's coefficient, H_{SO_2}, has been expressed with a proper equation that fits the experimental data (Maurer, 1980):

$$\ln H_{SO_2} = \frac{A}{T_{\text{d}}} + B\ln T_{\text{d}} + CT_{\text{d}} + D \tag{24}$$

A, B, C and D are species dependent coefficients.

The gas side mass transfer coefficient, $k_{\text{SO}_2,\text{g}}$, is evaluated with the modified Ranz–Marshall equation and the molecular diffusion coefficient, $D_{\text{SO}_2,\text{air}}$ is calculated with the Füller–Schettler–Giddings equation.

As for the evaporation of water, the partial pressure of SO_2 in the gas bulk is known from the solution of the corresponding gas phase species equation, while a dedicated chemical model has been developed for the evaluation of the dissolved sulphur dioxide concentration in the liquid bulk, $C_{SO_2,\infty}$.

4. Aqueous phase chemistry

In a wet limestone scrubbing system, a complex series of kinetic and equilibrium controlled reactions occur in the gas, liquid and solid phases. They may be stated in an overall expression as:

$$SO_{2(g)} + CaCO_{3(s)} + \frac{1}{2}O_{2(g)} + 2H_2O_{(aq)} \rightleftarrows CaSO_4 \cdot 2H_2O_{(s)} + CO_{2(g)} \tag{25}$$

This reaction can be divided in mainly five different steps, all of which occur simultaneously in the scrubber: absorption, neutralization, regeneration, oxidation and precipitation. The chemical model includes the reactions occurring in the spray zone, where the gas–liquid flow is analyzed. Therefore, regeneration, oxidation and precipitation processes are not considered further here because they mainly occur in the reaction tank (Marocco, 2008), as illustrated in Fig. 1.

The absorption and neutralization reactions can be assumed to be at equilibrium while a slurry droplet is inside the computational domain. These two equilibrium equations, together with water dissociation, a mass balance for the sulphur species, a mass balance for the carbon species and electroneutrality form a system of eight non-linear algebraic equations, in the eight unknown dissolved species concentrations $SO_{2,aq}$, $CO_{2,aq}$, H^+, OH^-, HSO_3^-, SO_3^{2-}, HCO_3^-, CO_3^{2-}, defining the droplet's liquid phase composition at each trajectory calculation step.

$$\begin{aligned}
K_{H_2O} &= (\gamma_\pm)^2[H^+][OH^-] \\
K_{SO_{2,aq}} &= (\gamma_\pm)^2\frac{[HSO_3^-][H^+]}{[SO_{2,aq}]} \\
K_{HSO_3^-} &= \gamma_\pm\frac{[SO_3^{2-}][H^+]}{[HSO_3^-]} \\
K_{CO_{2,aq}} &= (\gamma_\pm)^2\frac{[HCO_3^-][H^+]}{[CO_{2,aq}]} \\
K_{HCO_3^-} &= \gamma_\pm\frac{[CO_3^{2-}][H^+]}{[HCO_3^-]} \\
[C] &= [CO_{2,aq}] + [HCO_3^-] + [CO_3^{2-}] \\
[S] &= [SO_{2,aq}] + [HSO_3^-] + [SO_3^{2-}] \\
2[Ca^{2+}] - [Cl^-] &= [H^+] - [OH^-] - [HCO_3^-] \\
&\quad - 2[CO_3^{2-}] - [HSO_3^-] - 2[SO_3^{2-}]
\end{aligned} \tag{26}$$

The equilibrium constants of the reactions are evaluated with a temperature fit equation:

$$\ln K_i = \frac{A_i}{T} + B_i \ln T + C_i T + D_i \tag{27}$$

The species dependent parameters, A, B, C and D, are taken from the work of Maurer (1980) except the ones of the calcite solubility, K_{CaCO_3}, that derive from the work of Gage and Rochelle (1992).

The concentration of Ca^{2+} and Cl^- ions is predominant in the aqueous phase. Therefore, the multicomponent solution is assumed to be a single strong electrolyte solution of $CaCl_2$ and the modified form of the Debye–Hückel equation, proposed by Bromley (1972), is used to calculate the mean activity coefficient, $\gamma_\pm$.

The mass of all dissolved sulphur and carbon species and the concentration of calcium and chloride ions are all input parameters that must be provided to solve the set of equations.

At each droplet position inside the computational domain, the total dissolved sulphur species are calculated with Eq. (20), while the chloride concentration depends on process and economical

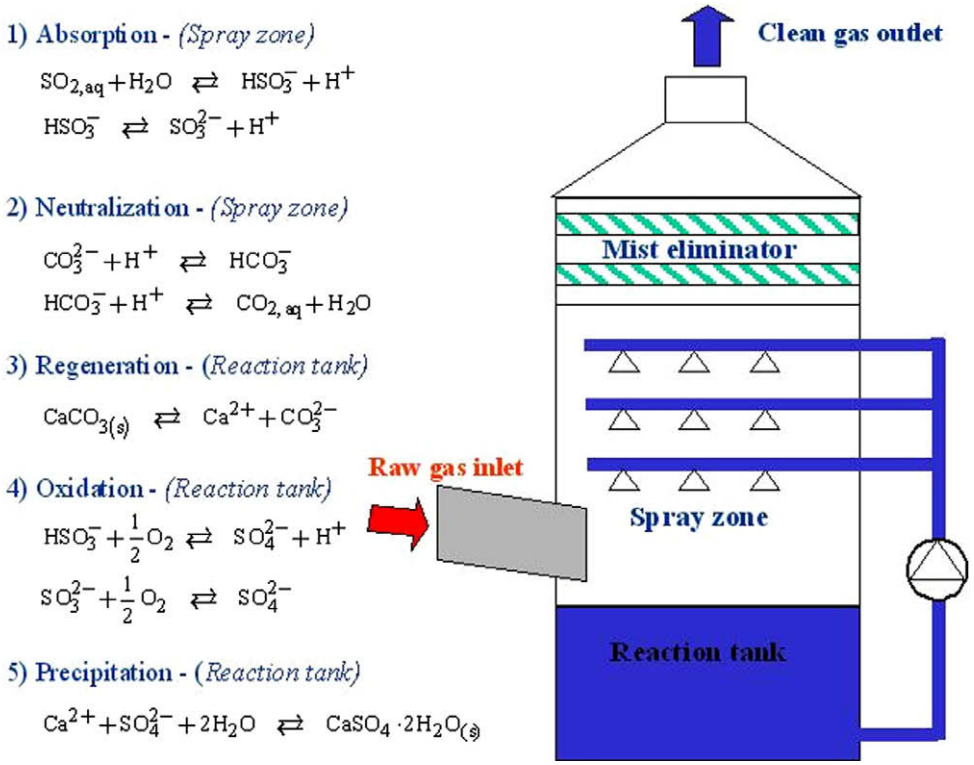

Fig. 1. Schematic picture of a WFGD scrubber along with the chemical reactions occurring inside of it.

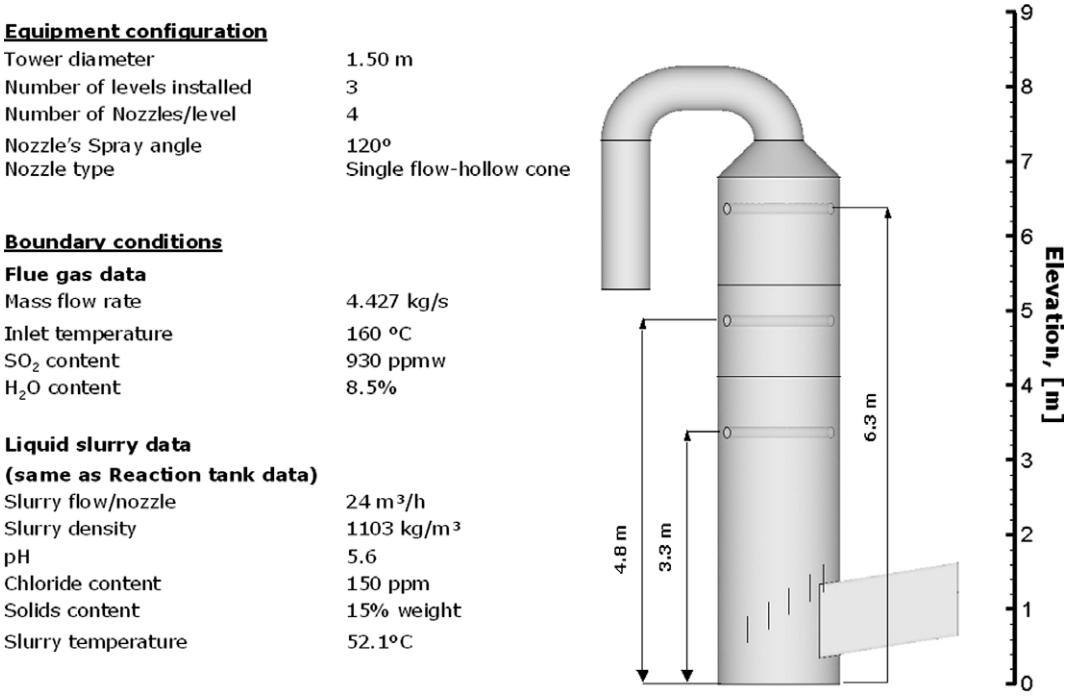

Fig. 2. Main geometrical and operating data of the simulated pilot plant.

considerations (Marocco, 2008). Because limestone dissolution and desorption of CO_2 into the gas phase are both neglected in the spray zone, calcium ions and total dissolved carbon species in a falling droplet are supposed to remain unchanged. Their evaluation at the injection of a droplet into the computational domain requires the solution of the following auxiliary system of chemical reactions for the four unknown dissolved species ($CO_{2,aq}$, HCO_3^-, CO_3^{2-}, Ca^{2+}) in the reaction tank, together with electroneutrality.

$$\begin{aligned} K_{CaCO_3} &= (\gamma_\pm)^2[Ca^{2+}][CO_3^{2-}] \\ K_{CO_{2,aq}} &= (\gamma_\pm)^2\frac{[HCO_3^-][H^+]}{[CO_{2,aq}]} \\ K_{HCO_3^-} &= (\gamma_\pm)\frac{[CO_3^{2-}][H^+]}{[HCO_3^-]} \\ [H^+]-[OH^-]-[Cl^-] &= 2[Ca^{2+}]-[HCO_3^-]-2[CO_3^{2-}] \end{aligned} \tag{28}$$

Chlorides are specified following the same considerations previously made, while the pH in the reaction tank, and thus the hydrogen and hydroxide ions concentration, $[H^+]$ and $[OH^-]$, is kept at a constant specified value that depends on process and economical considerations, (Marocco, 2008).

The solution of the non-linear systems of algebraic equations is obtained with a globally convergent Newton–Raphson method, as described by Dennis and Schnabel (1983). The implemented algorithm combines the rapid local convergence of a Newton's method with a globally convergent strategy that guarantees some progress towards the solution at each iteration.

5. Liquid-wall interaction

At present the simulation of a single impact phenomenon, considering also the interactions between splashed and impinging spray droplets, is very complex. Therefore, in a spray scrubber with many injection points the droplet-wall interaction has to be simulated through empirical correlations. The model here implemented is based on the experimental and numerical works of Weiss (2005) and Weiss and Wieltsch (2004), where they have studied coarse sprays, typical of flue gas scrubbing systems.

The droplet's rebound velocity, $\mathbf{v}_{reb}$, is related to the impact velocity, $\mathbf{v}_{imp}$, and the impact angle, α:

$$|\mathbf{v}_{reb}| = |\mathbf{v}_{imp}| - 0.04\alpha \tag{29}$$

The droplet's rebound angle, β, is related to the impact angle:

$$\beta = 0.002\alpha^2 + 0.06\alpha + 8.1 \tag{30}$$

In the equations above the velocities are expressed in [m/s] and the angles in [deg].

Weiss and Wieltsch have tested their liquid-wall interaction model in an experimental and numerical investigation of a pilot scrubber very similar to the one considered in the present work. They have found that the measured pressure drops were best predicted by an ideal reflection model, i.e. by the rebound of every droplet impacting onto the walls.

Accordingly, the present study uses the ideal reflection model for the numerical simulations of the pilot plant.

6. Pilot plant simulations

A pilot plant OST has been analyzed in CFD simulations and the results have been compared with the available experimental data.

The nozzles have not been geometrically modeled but they have been treated as slurry injection points. This simplification is justified by the negligible impact of their dimensions on the scrubber hydrodynamics compared to the other geometrical entities. Their presence would only significantly complicate the discretization of the domain. Locations, type and operating parameters are specified for each nozzle. When dealing with many injections and big computational domains, it is necessary to simplify the droplets' generation process. Thus the liquid flow ejected from the nozzles has been simulated as an ensemble of spherical droplets. The droplet size distribution has been reproduced by fitting the supplier's data through the *Rosin–Rammler* expression.

6.1. Flue gas properties

The flue gas flowing into the scrubber is a mixture of many species but only few of them significantly change their mass flow rate

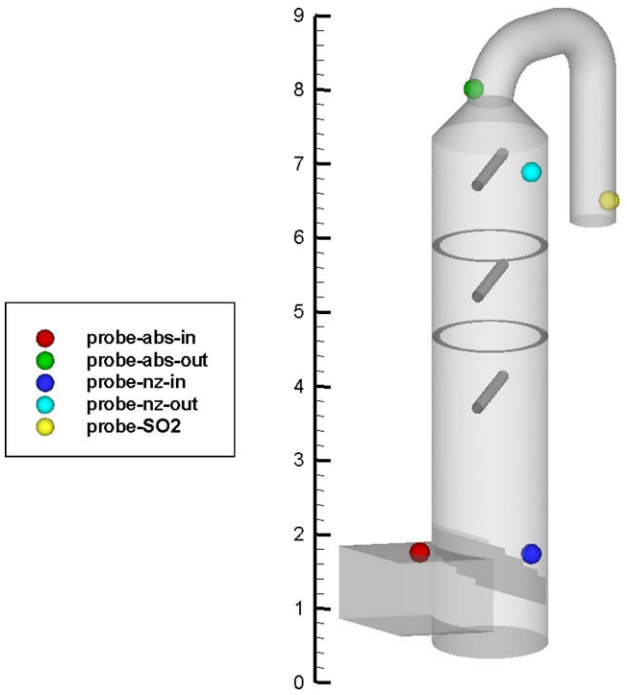

Fig. 3. Computational domain and location of the measuring probes.

across the tower. The gas phase is considered a *Newtonian mixture* of water vapor, sulphur dioxide and inert air and it obeys the perfect gas law.

Table 2
Finite volumes and injections data.

Finite volumes elements	
Coarse grid	
Number of control volume cells	700,000
Spray zone up to cone inlet	Tetrahedral
Cone and outlet duct	Hexahedral
Medium grid	
Number of control volume cells	1,577,094
Spray zone up to cone inlet	Tetrahedral
Cone and outlet duct	Hexahedral
Fine grid	
Number of control volume cells	3,392,167
Spray zone up to cone inlet	Tetrahedral
Cone and outlet duct	Hexahedral
Injections	
Number of injection points/nozzle	300
Number of diameter/injection point	10
Number of injected parcels/nozzle	3000
Total number of injected parcels/injection	36,000

The *flue gas density* and the *heat capacity* are functions of the mixture's temperature and composition. The *thermal conductivity* and the *viscosity* are constant all through the computational domain, while the *species mass diffusivities* in air have been calculated using the Füller–Schettler–Giddings correlation.

6.2. Slurry properties

The slurry droplets are considered a suspension of water, with dissolved species inside, and solids.

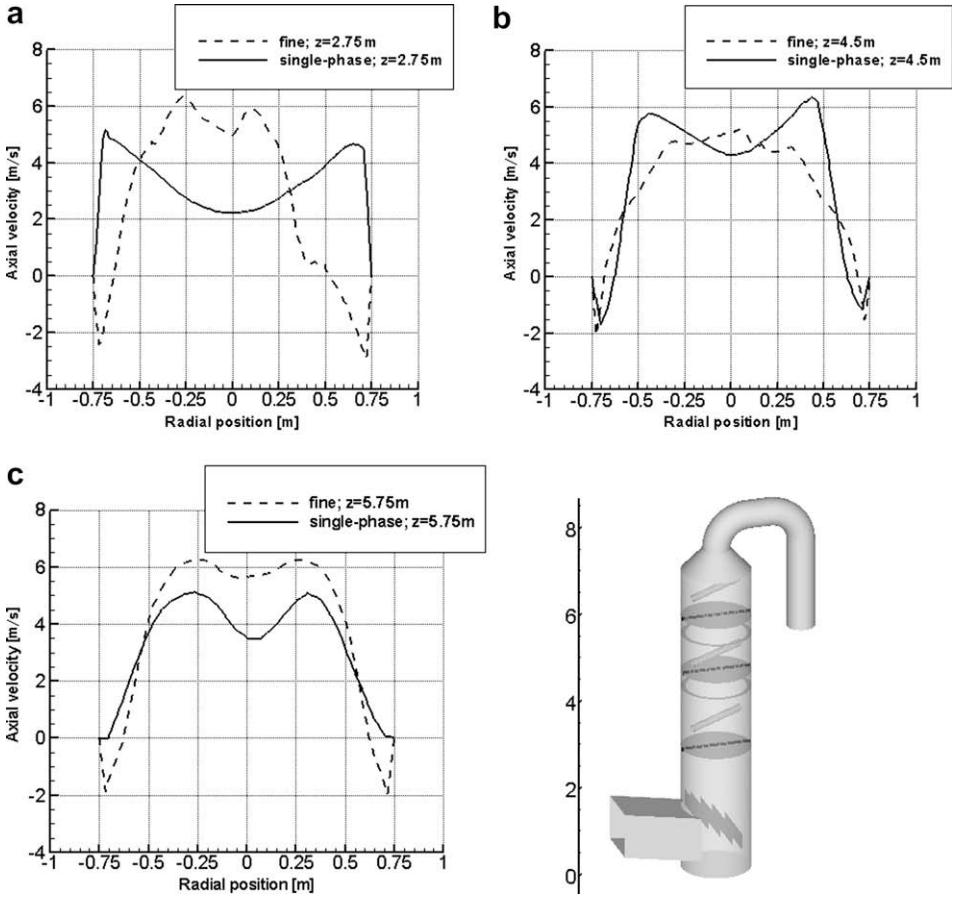

Fig. 4. Calculated axial velocity profiles for single- and two-phase flow on a line passing through scrubber center and normal to gas entrance, at three different elevations, respectively, at $z = 2.75$ m, $z = 4.5$ m and $z = 5.75$ m.

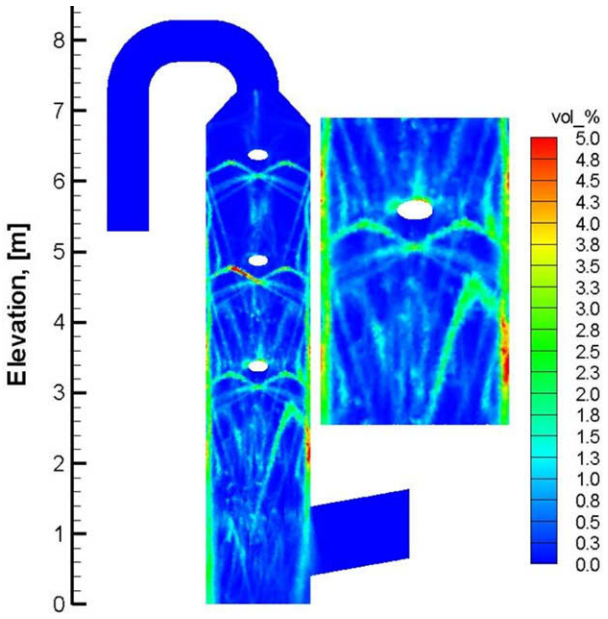

Fig. 5. Liquid volume fraction on a plane perpendicular to gas entrance; fine grid.

The *density of a droplet* can vary during the trajectory calculation due to evaporation. It is evaluated at every point in the domain by providing the solids mass fraction and the slurry density in the reaction tank, both related to process and economical considerations. The *droplet viscosity* has been assumed to vary with temperature as if it were water. The *specific heat* of a slurry droplet, c_d, has been assumed constant and equal to the specific heat of water at droplet's injection temperature.

6.3. Simulation results

The main geometrical dimensions of the pilot plant, together with the flue gas and slurry data, are summarized in Fig. 2.

Fig. 3 illustrates the absorber 3D geometry considered in the CFD simulation, together with the location of the measuring probes. A fan, located upstream of the scrubber, forces the raw gas to flow across the tower. The gas velocity is assumed to be homogeneously distributed over the inflow cross section. Five guide vanes are installed immediately downstream of the inlet duct to avoid the formation of a big flow recirculation in the zone opposite to the gas entrance.

Three different domain discretizations have been simulated. The number of discrete injected elements (parcels) has been gradually increased, in order to achieve a numerical independent solution from it. Table 2 summarizes the mesh and injections characteristics.

The velocity profile of the gas phase flowing alone across the scrubber is strongly modified by the presence of the slurry, as illustrated in Fig. 4. Hollow cone nozzles, with a wide opening angle of 120°, direct a substantial part of the injected liquid flow directly against the perimeter walls. According to the droplet-wall interaction model a liquid film forms so that the highest liquid volume fractions are located close to the walls, as shown in Fig. 5. The flue gas tends to by-pass this dense liquid region, where the velocity can be also directed downward, and is forced to move upward in the central part of the tower. This effect is more evident at the lowest measurement level, Fig. 4(a), where the liquid flow rate is higher, coming from all the three operating spray banks.

The dispersed liquid phase volume fraction reaches a maximum value of 5% inside the scrubber, as shown in Fig. 5. This justifies the fundamental assumption made of very dilute flow, $\alpha_d = 0$, for which particle–particle interaction and the effect of the particle volume fraction on the gas phase are negligible.

The flue gas flowing inside the scrubber cools down and increases its water content by exchanging heat and mass with the slurry droplets. It is known experimentally that saturation is reached very soon after the gas enters the tower. The simulated temperature and humidity fields agree with this observation, as illustrated in Fig. 6.

The SO_2 distribution field is shown in Fig. 7, where the sulphur dioxide removal efficiency is defined as $\eta_{SO_2} = 1 - \omega_{SO_2}(\mathbf{x})/\omega_{SO_{2,in}}$, being $\omega_{SO_{2,in}}$ and $\omega_{SO_2}(\mathbf{x})$ the SO_2 mass concentration at scrubber inlet and at a generic point inside the domain, respectively.

A convenient way of comparing the absorption rate for different conditions is to normalize the actual flux with respect to the maximal flux, i.e. the flux related to an infinite liquid side mass transfer coefficient. The *gas film resistance*, Θ, is defined as:

$$\Theta = \frac{1/k_g}{1/k_g + H/Ek_1^0} \tag{31}$$

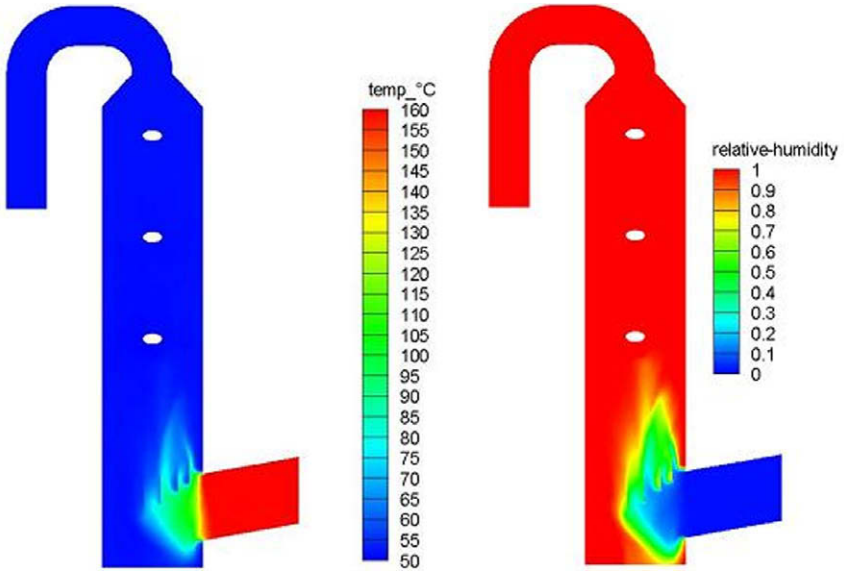

Fig. 6. Flue gas temperature and relative humidity on a plane perpendicular to gas entrance; slurry droplets injection temperature is 52.1 °C; fine grid.

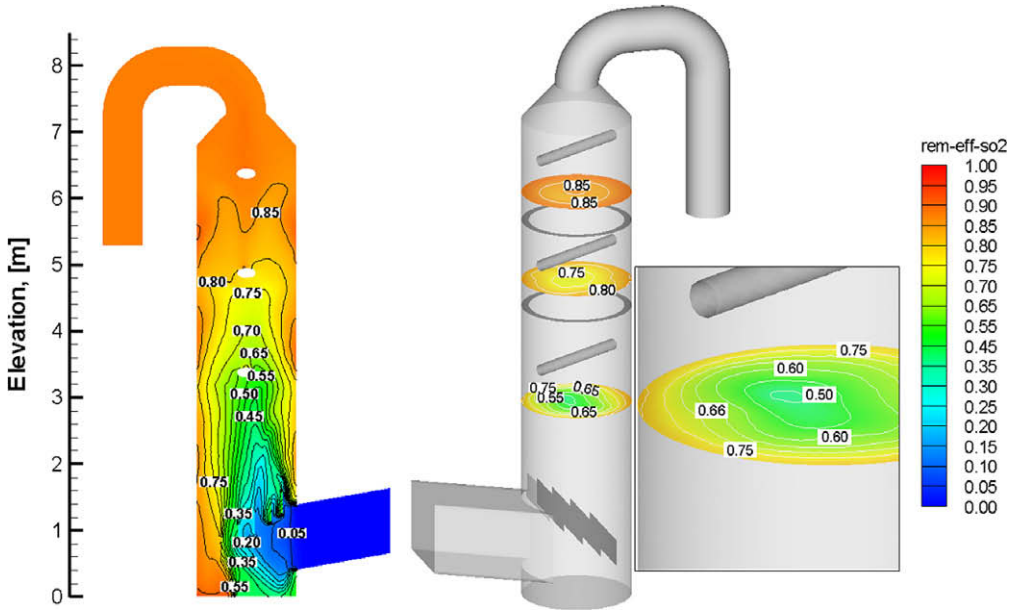

Fig. 7. SO_2 removal efficiency distribution on a plane perpendicular to gas entrance and on three horizontal planes at $z = 2.75$ m, $z = 4.5$ m and $z = 5.75$ m; fine grid.

For values of the gas film resistance close to unity, the absorption is "gas-film limited" and a further increase in the liquid side mass transfer rate will not enhance the absorption. If the gas film resistance is low the major part of the resistance to mass transfer is located in the liquid ("liquid-film limited"). Therefore, increasing the turbulence and/or the chemical reactivity of the slurry can enhance the absorption rate. The calculated values of the gas film resistance for a falling droplet, shown in Fig. 8, clearly indicate that the absorption of SO_2 within a spray scrubber is to a large extent liquid side limited.

The parameters that have been measured at the positions illustrated in Fig. 3 are pressure, temperature and sulphur dioxide concentration. The numerical results, computed at the same locations of the measuring probes, are in good agreement with the experimental data for all the parameters under observation, as shown in Fig. 9. The differences between the three domain discretizations are minor. The uncertainties of grid convergence have been analyzed with the Grid Convergence Index (GCI) method, based on Richardson extrapolation (Roache, 1994). The value of the GCI index represents a measure of the percentage difference between the numerical and the exact solution of the continuum equations, $GCI \propto (f_{num} - f_{exact})/f_{exact}$. The constraint for the applicability of the GCI method is verified in this study, i.e. the Taylor series expansion is valid asymptotically and the two grids are within the asymptotic range (Marocco, 2008).

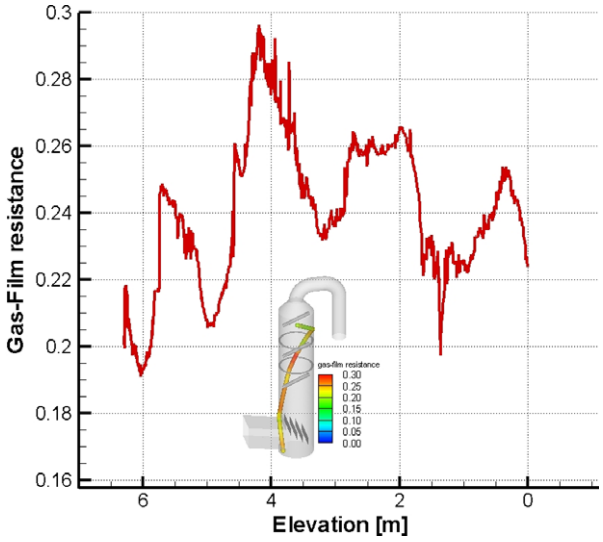

Fig. 8. Gas-film resistance of a falling droplet.

Table 3 summarizes the GCIs for the simulations of the pilot plant with the different grid discretizations. The GCI values of the fine and medium grid are acceptable for engineering purposes, i.e. the numerical solution is close enough to the exact solution. The only exceptions are the GCI values relative to the static pressure at absorber inlet and spray zone inlet (probe-abs-in and probe-nz-in of Fig. 3). This result is not amazing because both probes are located just before a sharp 90° bend and immediately after it, respectively. The high velocity gas flow coming from the inlet duct is forced to rapidly turn and to decelerate, which results in a high turbulence intensity in that region. To obtain a more accurate solution the grid should be further refined in that zone.

7. Conclusions

Today, the design of Open Spray Towers (OST) is essentially based on empirical and/or semi-empirical correlations that are only valid for a limited range of the design parameters, while the optimization of the fluid dynamics and chemistry of these equipments is necessary to comply with the stringent SO_2 emission requirements.

A model to calculate the absorption rate of sulphur dioxide into the droplets of limestone slurry has been developed and implemented into a commercial CFD code. Furthermore, besides SO_2 absorption, the model evaluates also the evaporation of slurry droplets and the droplet-wall interaction. Numerical simulations of a pilot plant have been performed on three different domain discretizations and the results have been compared with measured data. The uncertainties of grid convergence have been analyzed with the GCI method, which shows that the results obtained with the fine and medium grid are acceptable for engineering purposes. The spray zone inlet, where the high velocity flue gas enters into the OST, is the most critical to simulate. The discretization of this region should be carefully analysed, in order to obtain accurate solutions.

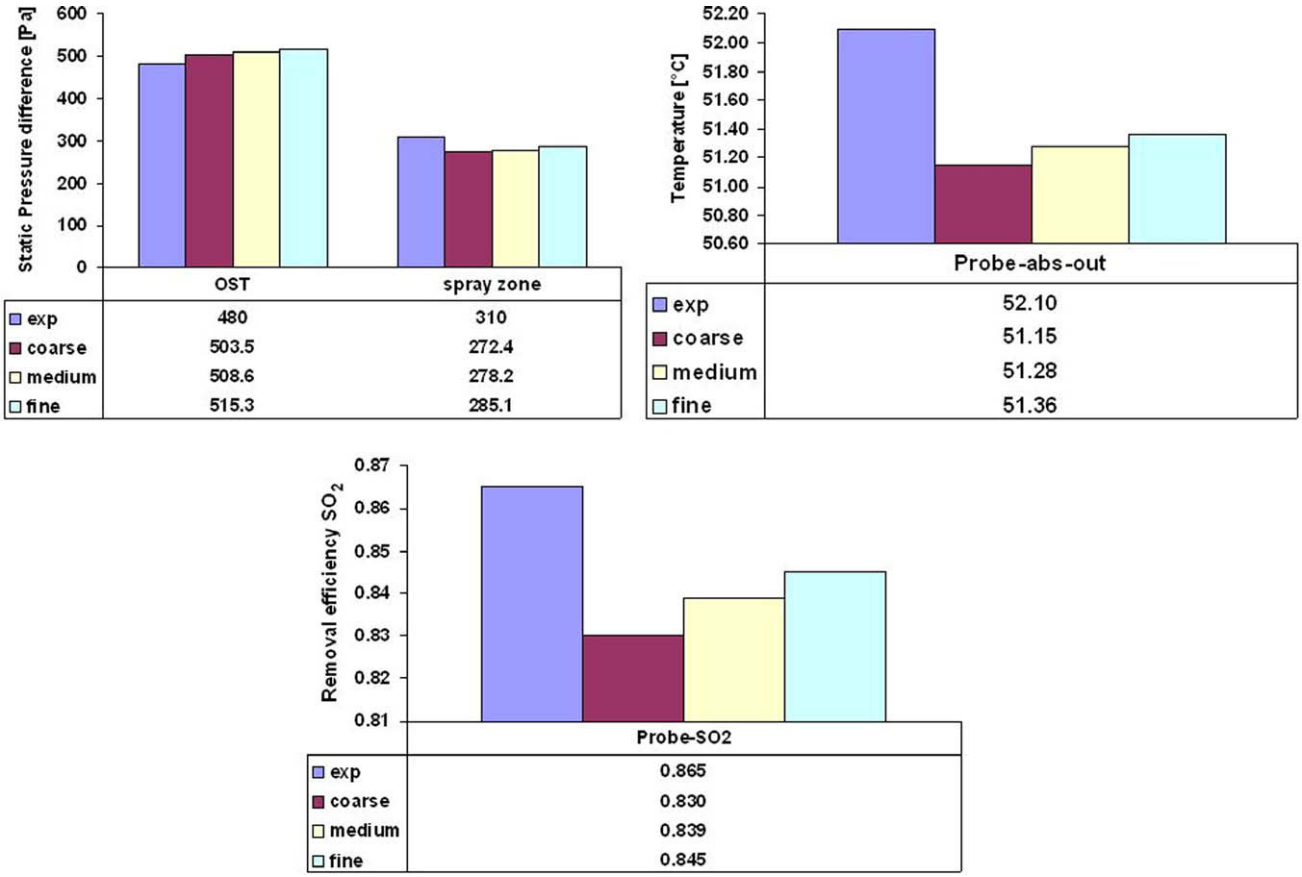

Fig. 9. Comparison between calculated and measured values of pressure drop, temperature and SO_2 removal efficiency. *OST* refers to the pressure difference between probe-abs-in and probe-abs-out; *spray zone* refers to the pressure difference between probe-nz-in and probe-nz-out.

Table 3
Grid Convergence Index (GCI) medium, GCI_{23}, and fine grid solutions, GCI_{12}.

	Coarse	Medium	Fine	GCI_{12}	GCI_{23}
Static pressure [Pa]					
Probe-abs-in	542.75	550.0	556.1	0.175	0.210
Probe-abs-out	39.245	41.381	40.77	0.0177	0.0615
Probe-nz-in	475.61	483.2	489.8	0.270	0.314
Probe-nz-out	203.16	205	205.2	0.00035	0.00328
Temperature [°C]					
Probe-abs-out	51.15	51.28	51.36	0.00747	0.01217
SO_2 removal efficiency					
Probe-SO_2	0.83	0.839	0.845	0.0426	0.0643

The flue gas is forced to flow upward in the central region of the OST where the liquid volume fractions are lower. This is more evident in the bottom part of the OST where the liquid flow rate is higher, coming from all operating spray levels. The use of nozzles with a wide spraying angle (120°) causes, accordingly to the droplet-wall interaction model applied, the highest liquid volume fractions to be located close to the perimeter walls. These values are anyway lower than 5%, which justify the fundamental assumption made of very dilute liquid phase, for which both particle–particle interaction and the effect of particle volume fraction on gas phase are negligible. While flowing inside the scrubber the flue gas is cooled and its relative humidity increases due to heat and mass exchange with the slurry droplets. It is experimentally observed that saturation is reached very soon after the gas enters the tower. The simulated humidity (temperature) field reflects well this observation.

The numerical values of pressure drop, flue gas temperature and SO_2 removal efficiency, calculated at the locations of the measuring probes, are in good agreement with the corresponding experimental data. FGD suppliers can then use the developed model in the design phase of industrial full-scale OST and for the retrofit of existing non-optimised equipments. Furthermore it allows considerable cost and time savings when used as a research tool instead of building a physical laboratory apparatus.

The model can also be extended to account for CO_2 desorption and natural oxidation of sulphite to sulphate due to the oxygen content in the flue gas. Furthermore the RSM may be a better approach than the k–ε model to turbulence simulation in gas–liquid flows.

Acknowledgement

The authors thank ALSTOM Power for providing the experimental data of the pilot plant.

References

Brogren, C., Karlsson, H.T., 1997. Modelling the absorption of SO_2 in a spray scrubber using the penetration theory. Chem. Eng. Sci. 52, 3085–3099.
Bromley, L.A., 1972. Approximate individual ion values of β (or B) in extended Debye–Hückel theory for uni-univalent aqueous solutions at 298.15 K. J. Chem. Thermodyn. 4, 669.
Crowe, C.T., Sommerfeld, M., Tsuji, Y., 1998. Multiphase Flow with Droplet and Particles. CRC Press, Boca Roton.
Dennis, J.E., Schnabel, R.B., 1983. Numerical Methods for Unconstrained Optimization and Nonlinear Equations. Prentice-Hall, Englewood Cliffs, NJ.
Gage, C.L., Rochelle, G.T., 1992. Limestone dissolution in flue gas scrubbing: effect of sulfite. J. Air Waste Manage. Assoc. 42, 926–935.
Heiting, B., Breuer, W., Bärnthaler, K., 2004. Erfahrungen bei der Inbetriebsetzung der REA im Kraftwerk Niederaussem, Block K. VGB Power Technol. 5, 93–99.

Hofelsauer, J., Notter, W., Marocco, L., Agalioti, M., Leoussis, P., 2008. Improvement of SO_2 removal with application of wall rings and advanced CFD modelling – the case of FGD unit Megalopolis. VGB Power Technol. 3, 85–89.

Klingspor, J.S., Cope, D.R., 1987. FGD Handbook. EA Coal Research, London.

Lapin, A., Lübbert, A., 1994. Numerical simulation of dynamics of two-phase gas flow in bubble columns. Chem. Eng. Sci. 49, 3661–3674.

Launder, B.E., Spalding, D.B., 1972. Lectures in Mathematical Models for Turbulence. Academic Press, London.

Marocco, L., 2008. Multiphase Euler-Lagrange CFD Study Applied to Wet Flue Gas Desulphurisation. PhD dissertation, Politecnico di Milano, Italy.

Maurer, G., 1980. On the solubility of volatile weak electrolytes in aqueous solutions. ACS Symp. Ser. 133, 139–172.

Morsi, S.A., Alexander, A.J., 1972. An investigation of particle trajectories in two-phase flow systems. J. Fluid Mech. 55, 193–208.

Perry, R.H., Green, Don.W., 1998. Chemical Engineers Handbook, seventh ed. McGraw-Hill, USA.

Poling, B.E., Prausnitz, J.M., O'Connel, J.P., 2001. The Properties of Gases and Liquids, fifth ed. McGraw-Hill, New York.

Ranz, W.E., Marshall Jr., W.R., 1952. Evaporation from drops – I and II. Chem. Eng. Prog. 48/3–48/4, 141–146. 173–180.

Roache, P.J., 1994. Perspective: a method of uniform reporting of grid refinement studies. ASME J. Fluids Eng. 116, 405–413.

Rowe, P.N., Claxton, K.T., Lewis, J.B., 1965. Heat and mass transfer from a single sphere in an extensive flowing fluid. Trans. Inst. Chem. Eng., 43.

Shih, T.H., Liou, W.W., Shabbir, A., Yang, Z., Zhu, J., 1995. A new k–ε Eddy–Viscosity Model for high Reynolds number turbulent flows – model development and validation. Comput. Fluids 24/3, 227–238.

Weiss, C., 2005. The liquid deposition fraction of sprays impinging vertical walls and flowing films. Int. J. Multiphase Flow 31, 115–140.

Weiss, C., Wieltsch, U., 2004. Laser optical flow measurements and computational fluid dynamic calculation of spray tower hydrodynamics. Chem. Eng. Res. Des. 83, 1–17.